J. Appl. Comput. Mech., 6(3) (2020) 640-652
DOI: 10.22055/JACM.2019.30309.1714

ISSN: 2383-4536
jacm.scu.ac.ir

M&MoCS

Shahid Chamran
University of Ahvaz

Journal of
Applied and Computational Mechanics

Research Paper

Effects of Non-uniform Suction, Heat Generation/Absorption and Chemical Reaction with Activation Energy on MHD Falkner-Skan Flow of Tangent Hyperbolic Nanofluid over a Stretching/Shrinking Eedge

A. Patra[1], M.K. Nayak[2], A. Misra[3]

[1] Department of Mathematics, Govt. Autonomous College, Rourkela, Odisha, India, Email: arunpatra58@gmail.com,

[2] Department of Physics, Radhakrishna Institute of Technology and Engineering, Bhubaneswar-752057, Odisha, India, Email: mkn2122@gmail.com

[3] Department of Mathematics, Centurion University of Technology and Management, Paralakhemundi, Gajapati-761211, Odisha, India, Email: amisra1972@gmail.com

Received July 14 2019; Revised September 24 2019; Accepted for publication September 24 2019.
Corresponding author: M.K. Nayak (manoj.nayak@riteindia.in)

Abstract. In the present investigation, the magnetohydrodynamic Falkner-Skan flow of tangent hyperbolic nanofluids over a stretching/shrinking wedge with variable suction, internal heat generation/absorption and chemical reaction with activation energy have been scrutinized. Nanofluid model is composed of "Brownian motion" and "Thermophoresis". Transformed non-dimensional coupled non-linear equations are solved by adopting the fourth-order R-K method along with the shooting technique. A comprehensive analysis of nanofluid velocity, the relative temperature, and its concentration profiles has been addressed. The major outcomes of the current study include that augmentation in the Weissenberg parameter, Hartmann number along with suction impede fluid flow and the shrinkage of the related boundary layer while internal heating develops an ascending thermal boundary layer for static and moving (stretching/shrinking) wedge. An increment in reaction rate undermines the nanoparticle concentration while that of activation energy exhibits a reverse trend.

Keywords: Falkner-Skan MHD Flow; Tangent Hyperbolic Nanofluid; Stretching/shrinking wedge; Variable Suction; Chemical Reaction with activation energy; Heat generation/absorption.

1. Introduction

Tangent hyperbolic fluids such as blood, ketchup, paint, whipped cream, and nail polish, etc. are a special class of non-Newtonian fluids that are characterized by eye-catching properties like simplicity, computational easiness, shear-thinning character, and physical robustness. Such fluids modify their flow properties subjected to operated shear stress. Because of the above advantages, tangent hyperbolic fluids are essentially used in several chemical engineering systems.

The study of nanofluids has been carried on by many scientists, engineers, and dynamic researchers because of their practical applications in the modern scientific world. Nanofluids are developed due to the suspension of nano-sized solid particles (metals such as aluminium, copper, iron and titanium and their oxides, carbides, or carbon nanotubes) in a base fluid (such as water, kerosene, oil, ethylene glycol, etc.). In the past, it has been experimentally proven that the addition of these ultrafine solid metal particles in base fluids contribute to a significant enhancement in the thermal conductivity [1]. As a result, it makes the fluid of high thermal conductivity which in turn makes them much proficient in heat transfer performance. Because of remarkable heat transfer performance (i.e., due to high thermal conductivity), the nanofluids are widely used in diversified fields of science and technology, like, thermal insulation, cancer therapy, asthma treatment, targeted drug release, elimination of tumors with hyperthermia, nuclear reactor cooling, power generation, etc. Later, Buongiorno [2] has carried on an investigation regarding the heat transport phenomenon in the flow of nanofluids. He proposed a seven-slip mechanism that plays a vital role in heat transfer enhancement. Further, he revealed that both thermophoresis and Brownian diffusion are the most suitable slip mechanisms for heat transfer enhancement. Further, many researchers investigated on the flow and heat transfer aspects of different nanofluids subject to varying conditions of motion.

The flow and heat transfer analysis a rectangular enclosure (Oztop and Nada [3]), stretched flow of nanofluids using first the Buongiorno model (Khan and Pop [4]), convective heat transfer in flow of nanofluids (Makinde and Aziz [5]), heat and mass transfer effects on stretched Carreau nanofluid flow (Hashim and Khan [6]), implementation of control volume based finite element method (CVFEM) to explore heat transfer characteristics of CuO nanofluids (Sheikholeslami [7]), transient squeezing flow of MHD nanofluid employing Duan-Rach Approach (Dogonchi et al. [8]) were analyzed. Recently, some interesting and motivational works on such aspects have been reported by many authors [9–17].

The present trend indicates that flows over wedge-shaped surfaces have extensive applications in the fields of hydrodynamics, aerodynamics, geothermal systems, heat exchangers, packed bed reactors, oil recovery, groundwater pollution, etc. [18-19]. Falkner and Skan [20] obtained the flow over a static wedge resulted in the development of the Falkner-Skan equation. In the past decades, many researchers have eventually contributed extraordinary eye-catching works on the Falkner-Skan flow in response to the impact of several thermophysical parameters. Later, Allan and Al Mdallal [21] obtained Series solutions of the modified Falkner-Skan equation, Watanabe [22] examined the behavior of forced flow over a wedge with uniform suction or injection and Ishak et al. [23] studied the MHD flow of a conducting fluid along with a moving wedge. Furthermore, the numerical study of MHD flow of γ Al2O3 nanofluids past a melting surface (Ganesh et al. [24]), MHD boundary layer stretched flow of tangent hyperbolic nanofluid (Akber et al. [25]) and impact of inclined Lorentz forces on tangent hyperbolic nanofluid flow (Prabhakar et al. [26]) were carried on successfully.

The reality is that the suction mechanism which significantly changes the flow field and regulates the thermal boundary layer structure in doing the jobs like adding reactants, reducing the drag, cooling the surface, preventing corrosion and creating an effective insulating layer in the flow domain. Su and Zheng [27] explored in their analysis that increment in fluid suction upsurges the velocity gradient in MHD Falkner-Skan flow thereby reducing the boundary layer thickness. Recently, the same observation was reported by Nayak [10]. Ganesh et al. [28] revealed that surface convection parameter in axisymmetric flow along a vertical stretching cylinder led to improve TBL. Further, Khan et al . [29] declared that increasing the values of thermal Biot number contributes to the heat transfer rate enhancement while the reverse trend is attained in the mass transfer rate. Heat generation has a key role in yielding thermal energy in the boundary layer leading to temperature rise while heat absorption causes the temperature to fall there. Heat generation/absorption is, therefore, an instrumental of the *HT* rate in the *TBL*. Ganga et al. [30] implemented the Buongiorno model to study the effect of internal heat generation/absorption on MHD flow of nanofluid subject to a plate.

The study of chemical reaction finds huge applications include pollution studies, processing of food, formation, and dispersion of fog, oxidation and synthesis materials, in the design of chemical processing equipments, biochemical engineering, plastic extrusion and metallurgy, supplies of moistures and temperature over an agricultural fairness and energy transfer in a drizzly cooling tower, etc. Mabood et al. [31] found that an increase in chemical reaction rate belittles nanoparticle volume concentration and exhibits the reverse trend with the rate of mass transfer in MHD stagnat ion point flow of nanofluids in a porous medium.

Recently, Khan et al. [32] studied the unsteady MHD Falkner-Skan flow of Carreau nanofluid over a static/moving wedge subject to convective boundary conditions influenced by the external magnetic field. However, they have not considered the tangent hyperbolic nanofluid, suction, heat generation/absorption and chemical reaction with activation energy in their investigation. In order to bridge the gap, the objective cum novelty of our present study is to investigate the MHD Falkner-Skan flow of tangent hyperbolic nanofluid past stretching/shrinking wedge under the influence of variable suction, heat generation/absorption and chemical reaction with activation energy. In the current study, the numerical solution of transformed governing equations is obtained by implementing the fourth-order R-K method along with the shooting technique. The effects of embedded parameters on the velocity, temperature, and nanoparticle concentration fields are displayed graphically and discussed literally.

2. Model Development

We consider a transient Falkner-Skan flow of an incompressible, electrical conducting tangent hyperbolic nanofluid over a stretching/shrinking wedge in response to an applied transverse magnetic field, variable suction, heat generation/absorption and chemical reaction with activation energy. Essentially, a small magnetic Reynolds number is chosen so that the induced magnetic field would be neglected. Again, the electric field is assumed to be absent. The moving wedge is considered permeable. A convective boundary condition is introduced in which the lower surface of the wedge receives heat through convection mechanism. Buongiorno model representing thermophoresis and

Brownian motion of nanoparticles are taken into account. We assume that the fluid flow is induced by a stretched velocity $u_w(x,t)$ and ambient velocity $u_e(x,t)$. Here $u_w(x,t)>0$ indicates a stretching wedge and $u_w(x,t)<0$ implicates a shrinking wedge (Fig.1). Let the wedge angle be $w=\beta\pi$. Further, we assume that (temperature, concentration) at the wedge surface (T_w, C_w) are higher than the ambient (temperature, concentration) i.e., (T_∞, C_∞) that is $T_w > T_\infty$ and $C_w > C_\infty$.

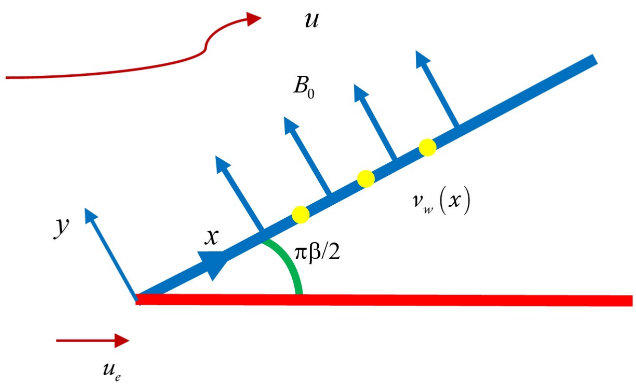

Fig. 1. Flow geometry.

The Falkner-Skan boundary layer flow is usually a viscous flow over a wedge (i.e., the flow in which the plate is not parallel to the flow) with free stream velocity $u_e(x)=\lambda x^n$, λ is a parameter (it may be a constant for steady flow or function of time for unsteady flow). This is the specificity of the Falkner-Skan flow compared to conventional flows.
With the help of the aforesaid assumptions and usual boundary layer theory, the continuity, Falkner-Skan momentum boundary layer equation, energy and concentration equations governing the unsteady chemically reactive tangent hyperbolic nanofluid wedge flow read [22, 23, 25,26]:

$$\frac{\partial u}{\partial x}+\frac{\partial v}{\partial y}=0 \tag{1}$$

$$\frac{\partial u}{\partial t}+u\frac{\partial u}{\partial x}+v\frac{\partial u}{\partial y}=\frac{\partial u_e}{\partial t}+u_e\frac{\partial u_e}{\partial x}+\upsilon(1-\varepsilon)\frac{\partial^2 u}{\partial y^2}+\sqrt{2}\upsilon\Gamma\varepsilon\frac{\partial u}{\partial y}\frac{\partial^2 u}{\partial y^2}-\frac{\sigma B_0^2}{\rho}(u-u_e) \tag{2}$$

$$\frac{\partial T}{\partial t}+u\frac{\partial T}{\partial x}+v\frac{\partial T}{\partial y}=\frac{k_f}{(\rho C_p)}\frac{\partial^2 T}{\partial y^2}+\tau\left[D_B\frac{\partial C}{\partial y}\frac{\partial T}{\partial y}+\frac{D_T}{T_\infty}\left(\frac{\partial T}{\partial y}\right)^2\right]+\frac{Q_0}{(\rho C_p)}(T-T_\infty) \tag{3}$$

$$\frac{\partial C}{\partial t}+u\frac{\partial C}{\partial x}+v\frac{\partial C}{\partial y}=D_B\frac{\partial^2 C}{\partial y^2}+\frac{D_T}{T_\infty}\frac{\partial^2 T}{\partial y^2}-k_r^2(C-C_\infty)\left(\frac{T}{T_\infty}\right)^m\exp\left(-\frac{E_a}{k_B T}\right) \tag{4}$$

The required boundary conditions are [26]:

(i) Static Wedge:

$$\left.\begin{aligned} u=0, v=v_w, -k\frac{\partial T}{\partial y}=h(T_w-T), C=C_w \quad at\ y=0 \\ u\to u_e,\ T\to T_\infty,\ C\to C_\infty \quad as\ y\to\infty \end{aligned}\right\} \tag{5}$$

(ii) Moving Wedge:

$$\left.\begin{aligned} u=u_w=\lambda u_e, v=v_w, -k\frac{\partial T}{\partial y}=h(T_w-T), C=C_w \quad at\ y=0 \\ u\to u_e,\ T\to T_\infty,\ C\to C_\infty \quad as\ y\to\infty \end{aligned}\right\} \tag{6}$$

where

$$\left.\begin{aligned} u_w(x,t) &= \frac{ax^n}{1-\delta t},\ v_w(x,t) = -S\sqrt{\left(\frac{n+1}{2}\right)\frac{\upsilon u_e}{x}} \\ T_w(x,t) &= T_\infty + \frac{T_0 u_w x}{\upsilon(1-\delta t)^{1/2}} \\ C_w(x,t) &= C_\infty + \frac{C_0 u_w x}{\upsilon(1-\delta t)^{1/2}} \\ u_e(x,t) &= \frac{bx^n}{1-\delta t} \end{aligned}\right\} \tag{7}$$

Here u and v are velocity components along x and y directions respectively, u_e is the free stream velocity, υ is the kinematic viscosity, ε is the material power law index, Γ is the material constant, σ is the electrical conductivity, B_0 is the uniform magnetic field strength, m is the Falkner-Skan power law parameter, $a>0$ stands for stretching wedge and $a<0$ stands for shrinking wedge. $\tau=(\rho C_p)_p/(\rho C_p)_f$ is the heat capacity ratio, $S>0$ represents suction. In Eq. (4), the term $k_r^2(T/T_\infty)^m\exp(-E_a/k_BT)$ represents the modified Arrhenius equation in which k_r^2 is the reaction rate. For the sake of similarity solutions, the stream function ψ is defined as $\psi(x,y,t)=\sqrt{2\upsilon x u_e/(n+1)}\ f(\eta)$ with $(u,v)=(\partial\psi/\partial y,-\partial\psi/\partial x)$ which identically satisfy Eq. (1). For the purpose the similarity transformations are:

$$\left.\begin{aligned} &u = u_e f'(\eta),\ v = -\sqrt{\left(\frac{n+1}{2}\right)\frac{\upsilon u_e}{x}}\left[f(\eta)+\left(\frac{n-1}{n+1}\right)\eta f'(\eta)\right] \\ &\theta(\eta) = \frac{T-T_\infty}{T_w-T_\infty},\ \phi(\eta)=\frac{C-C_\infty}{C_w-C_\infty},\ \eta = y\sqrt{\frac{(n+1)u_e}{2\upsilon x}} \end{aligned}\right\} \tag{8}$$

Using Eq. (8), Eqs. (2) - (6) become

$$\left[(1-\varepsilon)+\frac{\varepsilon}{\sqrt{2}}(2-\beta)Wef''\right]f'''+ff''+(\beta-1)f'f''+\beta\left(\frac{\eta}{2}f''-f'+1\right)-M(2-\beta)(f'-1)=0 \tag{9}$$

$$\theta''+\Pr(f\theta'-2f'\theta)+\Pr\left[Nb\theta'\phi'+Nt(\theta')^2+\frac{1}{2}(2-\beta)(Q\theta-A\eta\theta')\right]=0 \tag{10}$$

$$\phi''-\frac{\eta}{2}ASc(2-\beta)\phi'+Sc(f\phi'-2f'\phi)+\left(\frac{Nt}{Nb}\right)\theta''-2\Omega Sc\phi(1+\gamma\theta)^m\exp\left(-\frac{E}{1+\gamma\theta}\right)=0 \tag{11}$$

$$\left.\begin{aligned} &f'(0)=0,\ f(0)=S,\ \theta'(0)=-B_i[1-\theta(0)],\ \phi=1\ \ at\ \ \eta=0 \\ &f'\to 1,\ \theta\to 0,\ \phi\to 0\quad as\ \ \eta\to\infty \end{aligned}\right\}\ \text{(Static Wedge)} \tag{12}$$

$$\left.\begin{aligned} &f'(0)=+\lambda,\ f(0)=S,\ \theta'(0)=-B_i[1-\theta(0)],\ \phi=1\ \ at\ \ \eta=0\ \text{(Stretching wedge)} \\ &f'(0)=-\lambda,\ f(0)=S,\ \theta'(0)=-B_i[1-\theta(0)],\ \phi=1\ \ at\ \ \eta=0\ \text{(Shrinking wedge)} \\ &f'\to 1,\ \theta\to 0,\ \phi\to 0\quad \text{as}\ \ \eta\to\infty \end{aligned}\right\}\ \text{(Moving wedge)} \tag{13}$$

where

$$\begin{aligned} &M=\frac{\sigma B_0^2 x(1-\delta t)}{\rho u_e}, We=\sqrt{\frac{\left(\Gamma^2(n+1)^3u_e^3\right)}{2\upsilon x}},\ \beta=\frac{2n}{n+1},\ S=-\frac{v_w}{\sqrt{\left(\frac{n+1}{2}\right)\frac{\upsilon u_e}{x}}},\ \Pr=\frac{\upsilon}{\alpha}, N_t=\frac{\tau D_T(T_w-T_\infty)}{\upsilon T_\infty},\ E=\frac{E_a}{k_BT_\infty} \\ &N_b=\frac{\tau D_B(C_w-C_\infty)}{\upsilon}, Q=\frac{2Q_0x}{u_e(\rho C_p)}, A=\frac{\delta}{bx^{n-1}},\ \lambda=\frac{u_w}{u_e},\ Sc=\frac{\upsilon}{D_B},\ B_i=\frac{h}{k\sqrt{\frac{(n+1)u_e}{2\upsilon x}}},\ \Omega=\frac{xC_0k_r^2}{u_w},\ \gamma=\frac{T_w-T_\infty}{T_\infty} \end{aligned} \tag{14}$$

The local skin friction, Nusselt number and Sherwood number contribute the important characteristics of the flow. The local skin friction coefficient C_{fx} is expressed as:

$$C_{fx} = \frac{\tau_w(x)}{\rho u_w^2(x)} \tag{15}$$

where $\tau_w(x) = \mu_f[(1-\varepsilon)(\partial u/\partial y) + \varepsilon\Gamma(\partial u/\partial y)^2/\sqrt{2}]_{y=0}$ denotes the wall shear stress. The non-dimensional local skin friction coefficient can be presented in the form:

$$\lambda^{3/2}(2-\beta)^{1/2}\mathrm{Re}_x^{1/2}C_{fx} = \left[(1-\varepsilon) + \frac{\varepsilon}{2\sqrt{2}}(2-\beta)We\,f''(0)\right]f''(0) \tag{16}$$

The local Nusselt number is expressed as:

$$Nu_x = \frac{x\,q_w}{k(T_w - T_\infty)} \tag{17}$$

where $q_w = -k(\partial T/\partial y)_{y=0}$ denotes the wall heat flux. The non-dimensional local Nusselt number can be developed as:

$$\lambda^{1/2}(2-\beta)^{-1/2}Nu_x\,\mathrm{Re}_x^{-1/2} = -\theta'(0) \tag{18}$$

The local Sherwood number is expressed as:

$$Sh_x = \frac{x\,q_m}{D_B(C_w - C_\infty)} \tag{19}$$

where $q_m = -D_B(\partial C/\partial y)_{y=0}$ denotes the wall mass flux. The non-dimensional local Sherwood number can be developed as:

$$\lambda^{1/2}(2-\beta)^{-1/2}Sh_x\,\mathrm{Re}_x^{-1/2} = -\phi'(0) \tag{20}$$

where $\mathrm{Re}_x = x\,u_w(x)/\upsilon_f$ is the local Reynolds number.

3. Numerical Technique and Validation

A proficient Runge-Kutta fourth-order method along with the shooting technique has been applied to solve the coupled nonlinear ordinary differential equations (9) to (11) together with the boundary conditions (12) and (13). The deemed step size is $\Delta\eta = 0.01$. We repeat the process until we get the results correct up to the desired accuracy of 10^{-6} level. The numerical computations are executed for the non-dimensional parameters present in Eq. (9) to (13) and are presented in well appreciated graphical form. Table1 reflects the comparison with existing literature and found a good agreement with Ariel [33] and Srinivasacharya et al. [34].

4. Results and Discussions

The present study reports the transient flow and heat transfer behavior of chemically reactive tangent hyperbolic nanofluid past a static/moving wedge subject to stretching/shrinking condition under the influence of suction, heat generation/absorption and activation energy. The fourth-order R-K method along with shooting technique has been adopted to obtain the numerical solution of coupled non-linear equations. In the present study, we have explored the parametric effects of velocity, temperature and concentration profiles, respectively $f'(\eta)$, $\theta(\eta)$ and $\phi(\eta)$ using the results obtained from the comprehensive numerical computation. In the current study, $\lambda = 0$, $\lambda = 0.5$ and $\lambda = -0.5$ correspond to static wedge, stretching wedge and shrinking wedge respectively.

The field lines of the velocity field for different Weissenberg numbers (We) are displayed in Fig.2. For velocity profiles, facing its monotonic deceleration (up to $\eta = 2$) that is being visualized in the entire flow domain is due to strengthening of Weissenberg number We for all static and moving wedges (for both stretching and shrinking cases). However, the declining trend of velocity profiles is more pronounced for moving wedge in the shrinking case compared to the other two conditions of the wedge. As a result, the velocity boundary layer shrinks. It is true that Weissenberg number is the fluid relaxation time/viscous force. As We upsurges, relaxation time will be augmented. Larger relaxation time causes the fluid thicker which in turn provides more resistance to the fluid motion. Because of this, the fluid approaches from shear-thinning to shear thickening nature.

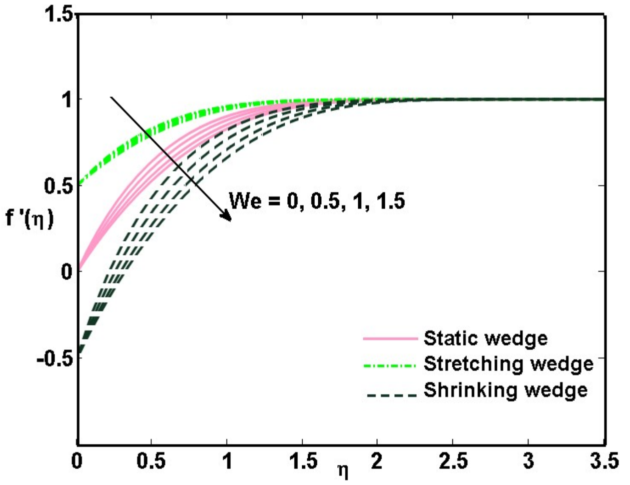

Fig. 2. Influence of Weissenberg number We on velocity profile when $\varepsilon = 0.5, \beta = 0.5, M = 0.4, S = 0.5$

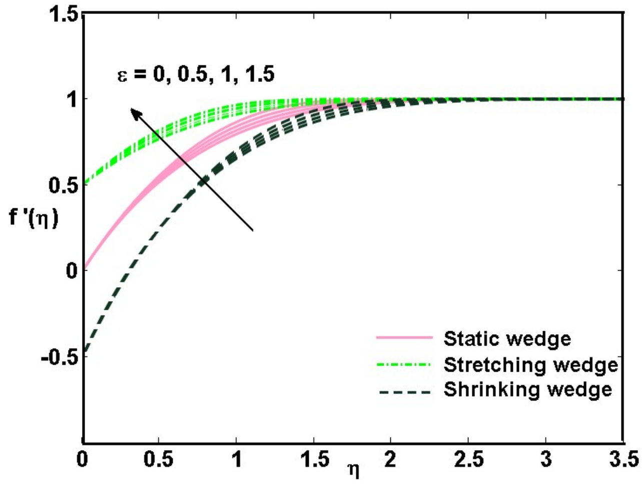

Fig. 3. Influence of material power law index ε on velocity profile when $\beta = 0.5, M = 0.4, S = 0.5, We = 1$

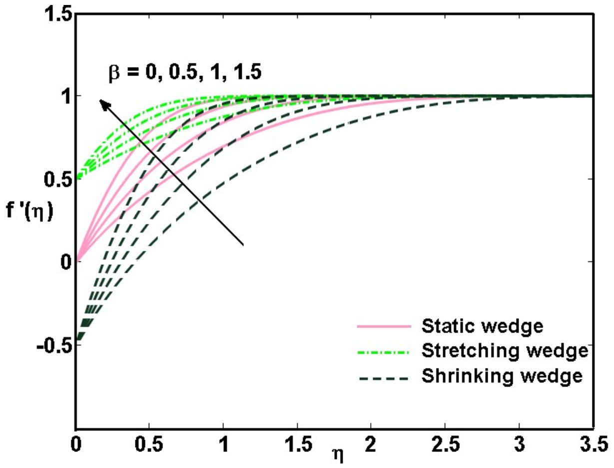

Fig. 4. Influence of wedge angle parameter β on velocity profile when $\varepsilon = 0.5, M = 0.4, S = 0.5, We = 1$

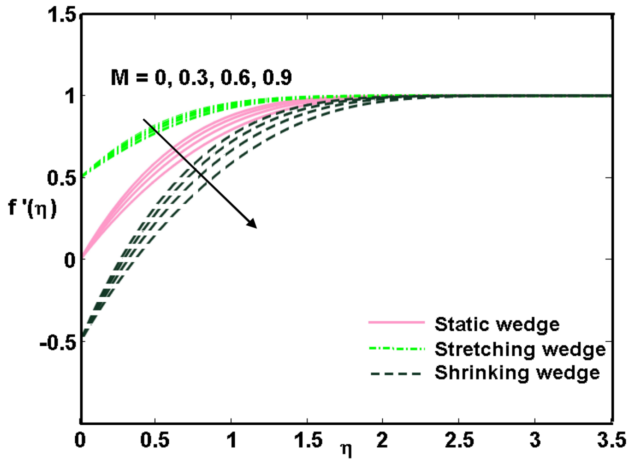

Fig. 5. Influence of Hartman number M on velocity when $\varepsilon = 0.5, \beta = 0.5, S = 0.5, We = 1$

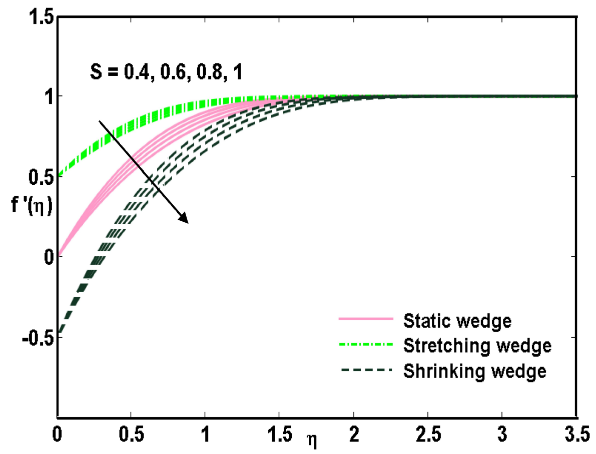

Fig. 6. Influence of S on velocity when $\varepsilon = 0.5, \beta = 0.5, M = 0.4, We = 1$

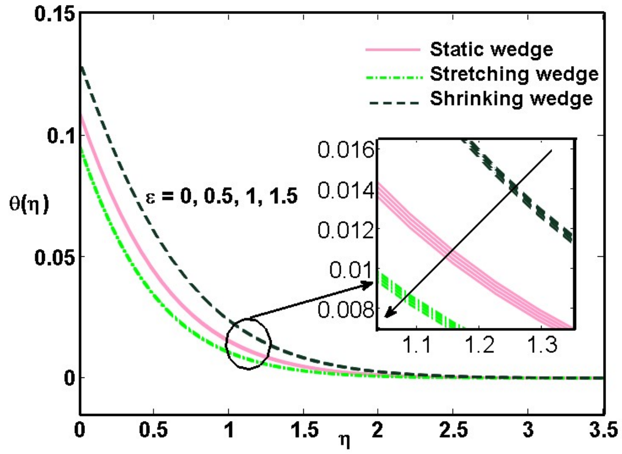

Fig. 7. Influence of ε on temperature when We=1, $\beta = 0.5,\ M = 0.4, Nt = 0.1,\ Nb = 0.1, \mathrm{Pr} = 1.2, A = 0.5,\ S = 0.5,$ $Bi = 0.2, Q = -2$

Notwithstanding the nature of the wedge (static/stretching/shrinking), the velocity field improves in increasing trend due to increasing values of power law index ε as is indicated in Fig. 3. Figure 4 demonstrates the impact of wedge angle parameter β on $f'(\eta)$ profiles for static, stretching and shrinking wedges. For each type of wedge, the fluid motion gets accelerated due to increment in β. However, the accelerating trend is prominent for a shrinking wedge compared to stretching and static wedges. As a result, an ascending velocity boundary layer is the result. Physically, wedge angle parameter accounts for pressure gradient. Hence, positive values of wedge angle parameter contribute to a favorable pressure gradient which in turn accelerates the flow. One important aspect of this observation is that $\beta = 0$ refers to wedge angle of zero degree indicating flow past a flat plate whereas $\beta = 0$ associated with wedge angle of 90° contributing to stagnation point flow.

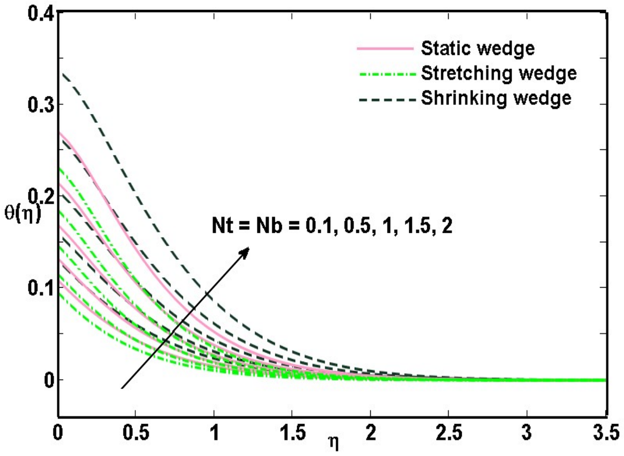

Fig. 8. The combined influence of Nb and Nt in temperature when $We = 1, \beta = 0.5, M = 0.4, \varepsilon = 0.5,$ $\Pr = 1.2, A = 0.5, S = 0.5, Bi = 0.2, Q = -2$

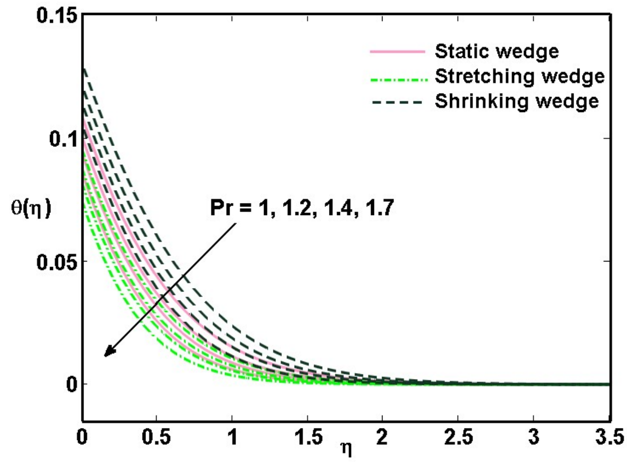

Fig. 9. Influence of Prandtl number Pr on temperature when $We = 1, \beta = 0.5, M = 0.4, \varepsilon = 0.5,$ $N_b = N_t = 0.1, A = 0.5, S = 0.5, Bi = 0.2, Q = -2$

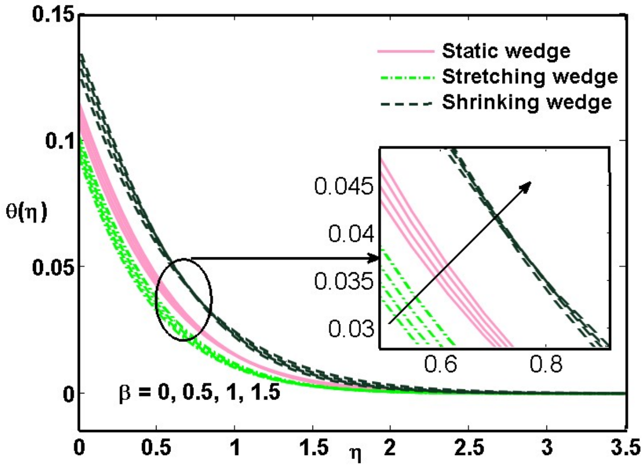

Fig. 10. Influence of wedge angle parameter β on temperature when $We = 1, \Pr = 1.2, M = 0.4, \varepsilon = 0.5,$ $N_b = N_t = 0.1, A = 0.5, S = 0.5, Bi = 0.2, Q = -2$

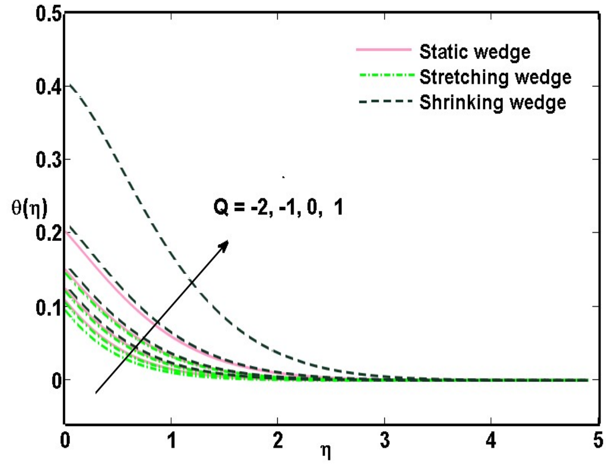

Fig. 11. Influence of heat generation/absorption parameter Q on temperature when $We = 1, \Pr = 1.2, M = 0.4, \varepsilon = 0.5,$ $N_b = N_t = 0.1, A = 0.5, S = 0.5, Bi = 0.2$

Figure 5 presents the behavior of Hartmann number M on velocity profile in which increases in M contributes diminutive fluid velocity $f'(\eta)$ for all static, stretching and shrinking wedges. Further, it has a like response (same trend) compared to the behavior of We on $f'(\eta)$. It is inferred from Fig. 6 the contribution of S on $f'(\eta)$ at fixed values of other pertinent parameters. The effect conveys that an increment in S declines the fluid velocity for static and moving (stretching/shrinking) wedge. The reason behind the persistent fall in fluid motion is just because of the role of suction that brings immeasurable quantities of ambient into the immediate neighborhood of the surface of the wedge.

Figures 7-11 inform the thermal behavior of the embedded parameters with respect to static, stretching and shrinking wedges. The influence of the material power law index ε on temperature profiles $\theta(\eta)$ is easily seen in Fig. 7. It is envisaged from this figure that an increment in ε peters the non-dimensional fluid temperature $\theta(\eta)$ out which in turn reduces the related boundary layer thickness in the flow domain. Figure 8 is the representation of $\theta(\eta)$ due to the combined influence of the Brownian motion parameter N_b and thermophoresis parameter N_t at specific values of other pertinent parameters. The non-dimensional fluid temperature $\theta(\eta)$ has been elevated with the rise of both N_b and N_t yielding the growth of the related boundary layer. The rationally behind such effective temperature growth is that an enhanced thermophoretic effect forces the nanoparticles of a hot surface to a cold ambient fluid.

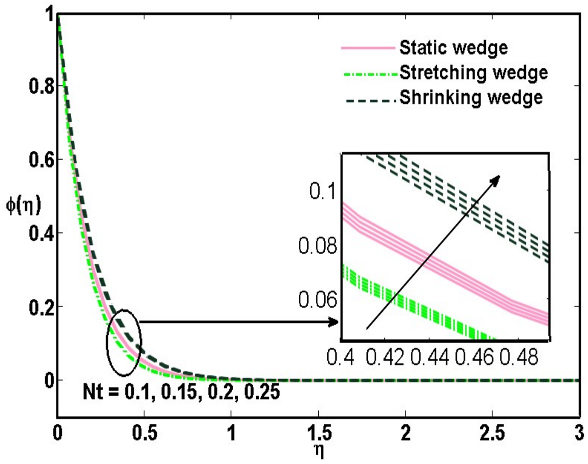

Fig. 12. Influence of thermophoresis parameter *Nt* on concentration when
$We=1, \Pr=1.2, \beta=0.5, M=0.4, \varepsilon=0.5, N_b=0.1,$
$Sc=5, E=1, \gamma=1, A=0.5, S=0.5, Bi=0.2, Q=-2$

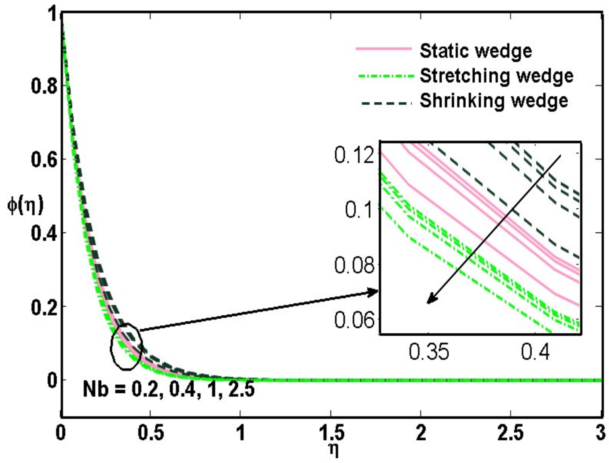

Fig. 13. Influence of Brownian motion parameter *Nb* on concentration when
$We=1, \Pr=1.2, \beta=0.5, M=0.4, \varepsilon=0.5, Nt=0.1,$
$Sc=5, E=1, \gamma=1, A=0.5, S=0.5, Bi=0.2, Q=-2$

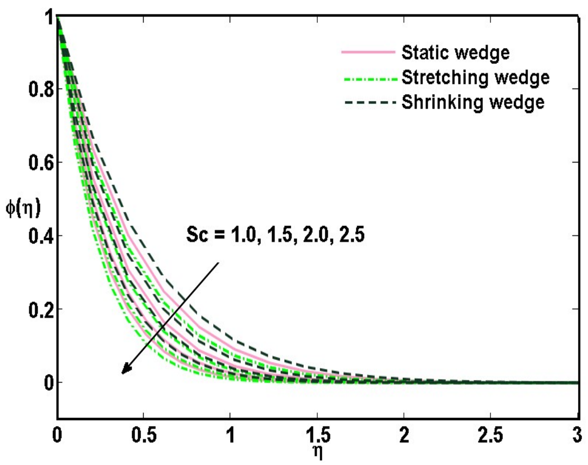

Fig. 14. Influence of Sc on concentration when
$We=1, \varepsilon=0.5, \beta=0.5, M=0.4, \gamma=1, Nb=0.1, Nt=0.1,$
$\Pr=1.2, \Omega=5, E=1, A=0.5, S=0.5, Bi=0.2, Q=-2$

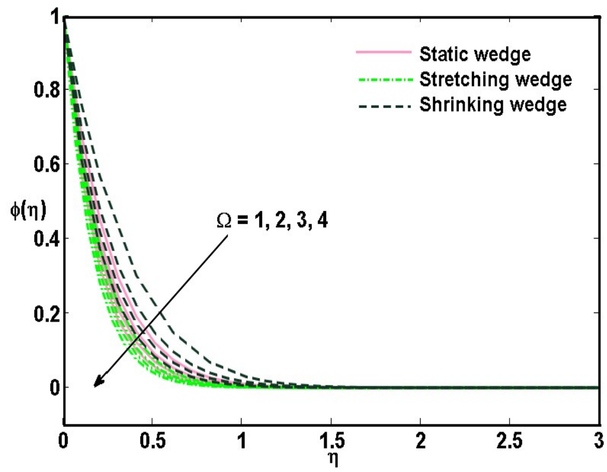

Fig. 15. Influence of Ω on concentration when
$We=1, \varepsilon=0.5, \beta=0.5, M=0.4, \gamma=1, Nb=0.1, Nt=0.1,$
$\Pr=1.2, Sc=5, E=1, A=0.5, S=0.5, Bi=0.2, Q=-2$

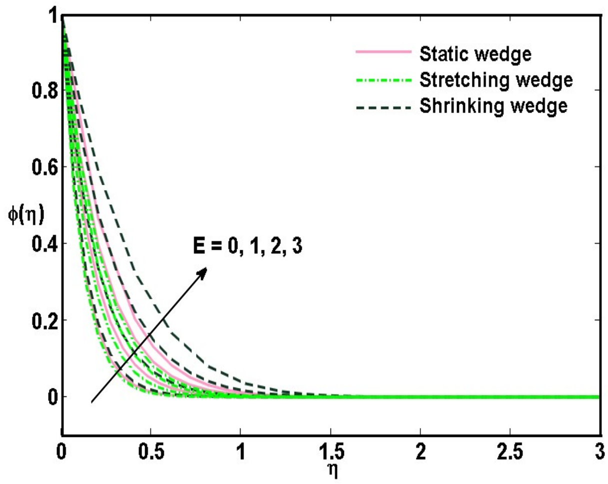

Fig. 16. Influence of dimensionless activation energy E on concentration when
$We=1, \varepsilon=0.5, \beta=0.5, M=0.4, \gamma=1, Nb=0.1, Nt=0.1,$
$\Pr=1.2, Sc=5, \Omega=5, A=0.5, S=0.5, Bi=0.2, Q=-2$

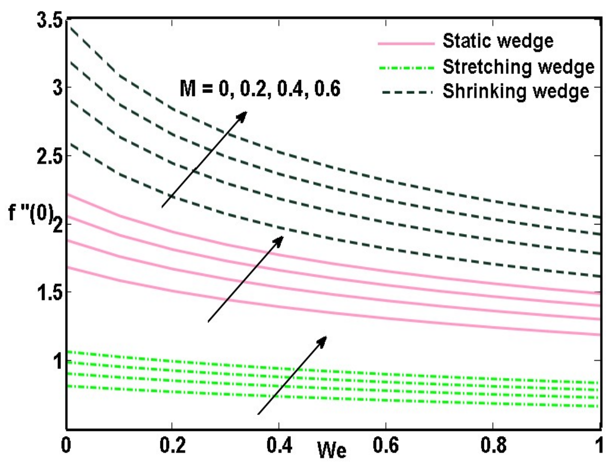

Fig. 17. Variation of $f''(0)$ with *We* for different *M*.

In terms of impact, Fig. 9 focuses the behavior of Prandtl number on temperature profiles where in all probability, the increase in Pr undermines the fluid temperature. The basic reason behind such decreasing trend of fluid temperature is that enhancing Pr weakens thermal diffusivity indicating less heat propagation into the fluid. Such an effect shrinks the thermal boundary layer. Next, Fig. 10 identifies the behavior of the wedge angle β on fluid temperature. It is a revelation that incremented β upsurges the non-dimensional fluid temperature in the entire flow region. In other words, if β had not been raised, the temperature profiles would have no options to build its increasing features. However, in the case of shrinking wedge, a transition occurs at $\eta = 0.7$ after which $\theta(\eta)$ exhibits the reverse trend. Furthermore, in the profiles of $\theta(\eta)$ shown in Fig. 11 it is envisioned that $\theta(\eta)$ upsurges due to an increase in heat generation parameter where the deviation is prominent for shrinking wedge compared to two other types of wedges.

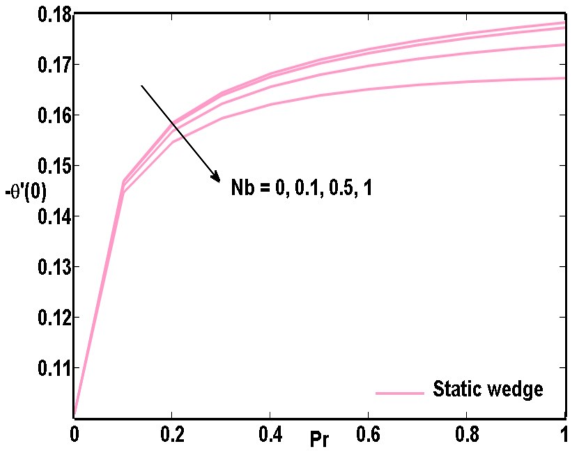

Fig. 18. Variation of $-\theta'(0)$ with *Pr* for different *Nb* for the static wedge.

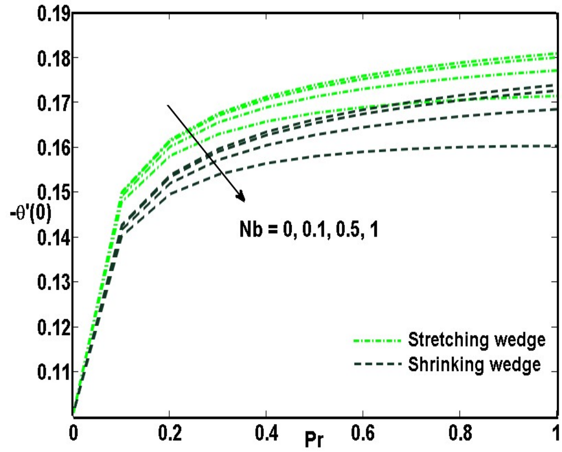

Fig. 19. Variation of $-\theta'(0)$ with *Pr* for different *Nb* for Stretching and Shrinking wedge.

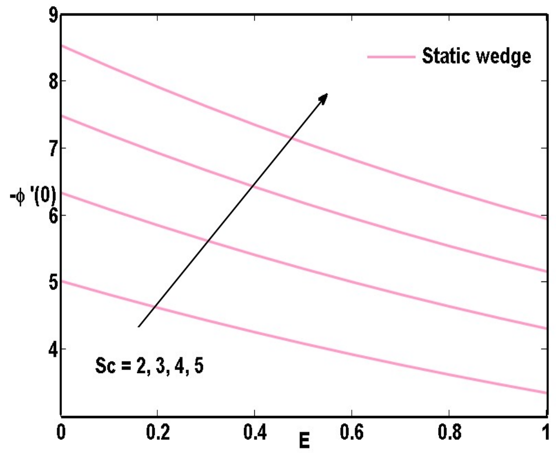

Fig. 20. Variation of $-\theta'(0)$ with *E* for different *Sc* for static wedge.

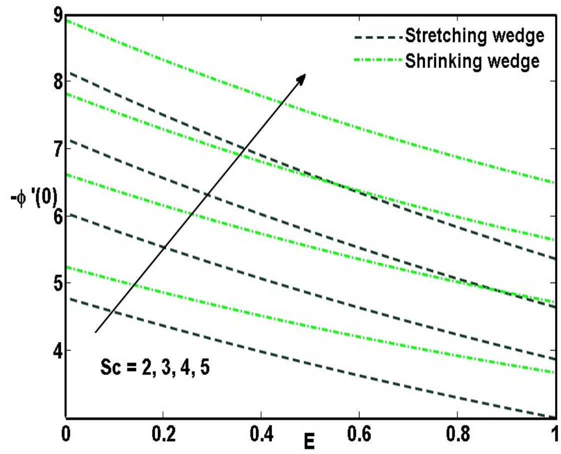

Fig. 21. Variation of $-\varphi'(0)$ with *E* for different Sc for stretching wedge and shrinking wedge.

It is clear from Figs. 12 and 13 that augmented Nt upsurges the nanoparticle concentration $\phi(\eta)$ while that of Nb exhibits the exact opposite trend. Figure 14 reveals the impact of the Schmidt number Sc on $\phi(\eta)$ profiles. In this context, the nature of impact is an increase in Sc belittles the $\phi(\eta)$ effectively throughout the flow domain. As a result, the concentration boundary layer shrinks. Fig. 15 illustrates the $\phi(\eta)$ profiles decline due to the enhancement of reaction rate Ω in the entire flow domain. However, the nanoparticle concentration $\phi(\eta)$ is expected to grow developing the related ascending boundary layer due to the increase in activation energy E (Fig. 16).

The impact of Lorentz force due to the applied magnetic field on skin friction $f''(0)$ for different values of the Wessienberg parameter We has been outlined in Fig. 17. It is viewed from this figure that wall shear stress upsurges appreciably due to enhancing the strength of the applied magnetic field. Figsures 18 and 19 reveal the behavior of Nb on heat transfer rate $-\theta'(0)$ affiliated with different values of Prandtl number Pr for static and moving (stretching/shrinking) wedges. It is well understood that increment in Nb enlarges the fluid temperature $\theta(\eta)$ which in turn undermines the heat transfer rate from the wedge leading to the narrowing of the thermal boundary layer. It is understood that fall in heat transfer rate is prominent in case of moving wedge (Stretching/Shrinking) compared to static wedge. Nevertheless, the nature of the wedge static or moving (stretching/shrinking), heat transfer diverges much much more away from the wedge surface. Figsures 20 and 21 convey about the variation of Sherwood number (mass transfer rate) for varying values of activation energy E under the influence of increasing Schmidt number Sc. The reality is that Schmidt number is the ratio of kinematic viscosity to molecular diffusivity. therefore, It implicates that increase in Sc weakens molecular diffusivity thereby undermining nanoparticle concentration yielding more mass transfer rate from the wedge surface for both static and moving (stretching/shrinking) wedge. Amazingly, it is seen that mass transfer is attained at faster rate for shrinking wedge compared to by wedge under the impact of different strength of activation energy (Fig. 21).

Table 1 enlists the numerical value of $f''(0)$ for different magnetic parameter M. A close observation to it reveals that incremented magnetic field strength leads to an augmentation of the wall shear stress. This is in excellent agreement with the reports provided earlier by noteworthy researchers Ariel [33] and Srinivasacharya et al. [34].

Table 1. Comparison of $f''(0)$ calculated by the present method and that of Ariel [33] and Srinivasacharya et al. [34] for $\varepsilon=0,\ \beta=1,\ We=0,\ Nb=0,\ Nt=0,\ A=0,\ Q=0,\ Sc=0.24,\ \Omega=0,\ \gamma=1,\ m=0.5,\ E=1,\ \lambda=0,\ Bi=-1,\ S=0$.

M	Ariel [28]	Srinivasacharya et al. [29]	Present
0	1.232588	1.232597	1.218724
1	1.585331	1.585280	1.569303
4	2.346663	2.346870	2.332235
25	5.147965	5.147965	5.140185
100	10.074741	10.074741	10.070646

5. Conclusion

In the present article, it has been focused on the MHD flow of hyperbolic tangent nanofluid subject to variable suction, internal heat absorption/generation, chemical reaction and activation energy past a stretching/shrinking wedge. An intensive study of the current problem has conveyed the following major outcomes:

- Augmented Weissenberg number provides a decline in the velocity profile of static, stretching and shrinking sheets until a stable state is attained.
- To be fair, the increase in material power law index ε and wedge angle parameter β amplified the fluid velocity with superior values for the shrinking wedge.
- Enhanced magnetic field strength and fluid suction establish diminutive velocity fields and the related descending boundary layer.
- An increment in reaction rate belittles the nanoparticle concentration while that of activation energy exhibits a reverse trend.

Our results convey the readers an insight to understand the combined influence of Brownian diffusion and thermophoretic force on the heat transfer rate. This study can provide a benchmark to accelerate the experimental studies in this domain (Sadri et al. [35]).

Author Contributions

A. Patra planned the scheme and initiated the project. M.K. Nayak developed the mathematical modeling and carried on the simulation. A. Misra analyzed the empirical results and examined the theory validation. The manuscript was written through the contribution of all authors. All authors discussed the results, reviewed and approved the final version of the manuscript.

Conflict of Interest

The authors declared no potential conflicts of interest with respect to the research, authorship, and publication of this article.

Funding

The authors received no financial support for the research, authorship, and publication of this article.

Nomenclature

T_∞ Ambient fluid temperature

C_∞ Ambient particle concentration

E_a Activation energy

B_i	Biot's number
k_B	Boltzmann constant
D_B	Brownian diffusion coefficient
N_b	Brownian motion parameter
a, b, δ ,n	Constants
ρ	Density of fluid
Ω	Dimensionless reaction rate
μ	Dynamic viscosity of fluid
B_0	External magnetic field imposed
σ	Electrical conductivity
m	Fitted rate constant
T	Fluid temperature within the boundary layer
T_w	Fluid temperature on the surface of the wedge
$u_e(x)$	Free stream velocity
HT	Heat transfer
Q	Heat generation/absorption parameter
ρC_p	Heat capacitance of base fluid
M	Hartmann number
h	Heat transfer coefficient
$(T_{0,} C_0)$	Initial reference (fluid temperature, particle concentration)
υ	Kinematic viscosity
Re_x	Local Reynolds numbers
Γ	Material constant
$\in$	Material power law index
E	Non-dimensional activation energy
$f'(\eta)$	Non-dimensional velocity
$\theta(\eta)$	Non-dimensional temperature
$\phi(\eta)$	Non-dimensional particle concentration
η	Non-dimensional vertical distance
C	Particle concentration within the boundary layer
C_w	Particle concentration on the surface of the wedge
Pr	Prandtl number
Q_0	Rate of heat generation/absorption
S	Suction parameter
Sc	Schmidt number
$v_w(x,t)$	Suction velocity
γ	Temperature ratio parameter
TBL	Thermal boundary layer
TC	Thermal conductivity
k	Thermal conductivity
N_t	Thermophoresis parameter
D_T	Thermophoretic diffusion coefficient
B_0	Uniform magnetic field strength
A	Unsteadiness parameter
(u, v)	Velocity components in (x, y) directions
λ	Velocity ratio parameter
q_w	Wall heat flux
q_m	Wall mass flux
β	Wedge angle parameter
We	Weissenberg number

Subscripts

f	Fluid
p	Particle
w	Quantities at wall
∞	Quantities at free stream

Reference

[1] Choi S.U.S., Enhancing thermal conductivity of fluids with nanoparticles, *ASME Fluids Eng. Division*, 231, 1995, 99-105.
[2] Buongiorno, J., Convective transport in nanofluids, *J. Heat Transf.*, 128(3), 2006, 240–250.
[3] Oztop H.F., Nada E.A., Numerical study of natural convection in partially heated rectangular enclosures filled with nanofluids, *Int. J. Heat Fluid Flow*, 29(5), 2008, 1326–1336.
[4] Khan W., Pop I., Boundary-layer flow of a nanofluid past a stretching sheet, *Int. J. Heat Mass Transf.*, 53, 2010, 2477–2483.
[5] Makinde O.D., Aziz A., Boundary layer flow of a nanofluid past a stretching sheet with a convective boundary condition, *Int. J. Therm. Sci.*, 50, 2012, 1326–1332.
[6] Khan Hashim M., A revised model to analyze the heat and mass transfer mechanisms in the flow of Carreau nanofluids, *Int. J. Heat Mass Transf.*, 103, 2016, 291–297.
[7] Sheikholeslami M., Vajravelu K., Rashidi M.M., Forced convection heat transfer in a semi annulus under the influence of a variable magnetic field, *Int. J. Heat Mass Transf.*, 92, 2016, 339–348.
[8] Dogonchi A.S., Divsalar K., Ganji D.D., Flow and heat transfer of MHD nanofluid between parallel plates in the presence of thermal radiation, *Comp. Math. Appl. Mech. Eng.*, 310, 2016, 58–76.
[9] Nayak M.K., Akbar N.S., Pandey V.S., Khan Z.H., Tripathi D., 3D free convective MHD flow of nanofluid over permeable linear stretching sheet with thermal radiation, *Powd. Technol.*, 315, 2017, 205-215.
[10] Nayak M.K., Chemical reaction effect on MHD viscoelastic fluid over a stretching sheet through porous medium, *Meccanica*, 51, 2016, 1699-1711.
[11] Aman S., Khan I., Ismail Z., Salleh M.Z., Al-Mdallal Q. M., Heat transfer enhancement in free convection flow of CNTs Maxwell nanofluids with four different types of molecular liquids, *Scientific Reports*, 7(1), 2017, 2445-2455.
[12] Nayak M.K., Akbar N.S., Pandey V.S., Khan Z.H., Tripathi D., MHD 3D free convective flow of nanofluid over an exponentially stretching sheet with chemical reaction, *Adv. Powder Technol.*, 28(9), 2017, 2159-2166.
[13] Nayak M.K., Shaw S., Chamkha A.J., MHD free convective stretched flow of a radiative nanofluid inspired by variable magnetic field, *Arab. J. Sci. Eng.*, 44(2), 2019, 1269-1282.
[14] Besthapu P., Haq R.U., Bandari S., Al-Mdallal Q.M., Thermal radiation and slip effects on MHD stagnation point flow of non-Newtonian nanofluid over a convective stretching surface, *Neural Compt. Appl.*, 31(1), 2019, 207-217.
[15] Khan Z.H., Qasim M., Haq R. U., Al-Mdalla Q.M., Closed-form dual nature solutions of fluid flow and heat transfer over a stretching/shrinking sheet in a porous medium, *Chinese J. Physics*, 55(4), 2017, 1284-1293.
[16] Nayak M.K., MHD 3D flow and heat transfer analysis of nanofluid by shrinking surface inspired by thermal radiation and viscous dissipation, *Int. J. Mech. Sci.*, 125, 2017, 185-193.
[17] Nayak M.K., Mehmood R., Makinde O.D., Mahian O., Chamkha A.J., Magnetohydrodynamic flow and heat transfer impact on ZnO-SAE50 nano lubricant flow due to an inclined rotating disk, *J Central South University*, 26, 2019, 1146-1160.
[18] Schlichting H., Gersten K., Boundary layer theory, 8th ed. *Springer-Verlag*, Berlin, 2000.
[19] Leal L.G., Advanced transport phenomena: Fluid mechanics and convective transport processes, *Cambridge Univ. Press*, New York, 2007.
[20] Falkner V.M., Skan S.W., Some approximate solutions of the boundary-layer equations, *Philos. Mag.*, 12, 1931, 865–896.
[21] Allan, Q.M., Al Mdallal, Q.M., Series solutions of the modified Falkner-Skan equation, *Int. J. Open Probl. Compt. Math.*, 4(2), 2011, 189-198.
[22] Watanabe T., Thermal boundary layers over a wedge with uniform suction or injection in forced flow, *Acta Mech.*, 83(3), 1990, 119–126.
[23] Ishak A., Nazar R., Pop I., MHD boundary-layer flow past a moving wedge, *Magnetohydrodynamics*, 1, 2009, 103–110.
[24] Ganesh N.V., Al-Mdallal Q.M., Kameswaran P.K., Numerical study of MHD effective Prandtl number boundary layer flow of γ Al2O3 nanofluids past a melting surface, *Case Studies Thermal Eng.*, 13, 2019, 100413.
[25] Akbar N.S., Nadeem S., Haq R.U., Khan Z.H., Numerical solutions of Magneto-hydrodynamic boundary layer flow of tangent hyperbolic fluid towards a stretching sheet, *Indian J. Phys.*, 87, 2013, 1121–1124.
[26] Prabhakar B., Bandari S., Haq R.U., Impact of inclined Lorentz forces on tangent hyperbolic nanofluid flow with zero normal flux of nanoparticles at the stretching sheet, *Neural Comput. Appl.*, DOI 10.1007/s00521-016-2601-4.
[27] Su X., Zheng L., Approximate solutions to MHD Falkner-Skan flow over permeable wall, *Appl. Math. Mech.*, 32(4), 2011, 401–408.

[28] Ganesh N.V., Ganga B., Abdul Hakeem A.K., Saranya S., Kalaivanan V.R., Hydromagnetic axis-symmetric slip flow along a vertical stretching cylinder with convective boundary condition, *St. Petersburg Polyt. University J: Phys. and Math.,* 2, 2016, 273–280.
[29] Khan M., Azam M., Alshomrani A.S., On unsteady heat and mass transfer in Carreau nanofluid flow over expanding or contracting cylinder with convective surface conditions, *J. Mol. Liq.*, 231, 2017, 474-484.
[30] Ganga B., Ansari S.M.Y., Ganesh N.V., Hakeem A.K.A., MHD flow of Boungiorno model nanofluid over a vertical plate with internal heat generation/absorption, *Propul. Power Research*, 5(3), 2016, 211-222.
[31] Mabood F., Shateye S., Rashidi M.M., Momoniat E., Freidoonimehr N., MHD stagnation point flow heat and mass transfer of nanofluids in porous medium with radiation, viscous dissipation, and chemical reaction, *Adv. Powder Technol.*, 27, 2016, 742-749.
[32] Khan M., Azam M., Munir A., On unsteady Falkner-Skan flow of MHD Carreau nanofluid past a static/moving wedge with convective surface condition, *J. Mol. Liq.*, 230, 2017, 48-58.
[33] Ariel P.D., Hiemenz flow in hydromagnetics, *Acta Mech*., 103, 1994, 31–43.
[34] Srinivasacharya D., Mendu U., Venumadhav K., MHD boundary layer flow of a nanofluid past a Wedge, *Procedia Eng.,* 127, 2015, 1064–1070.
[35] Sadri R., Ahmadi G., Togun H., Dahari M., Kazi S.N., Sadeghinezhad E., Zubir N., An experimental study on thermal conductivity and viscosity of nanofluids containing carbon nanotubes. *Nano. Res. Lett.,* 9(1), 2014, 151.

ORCID iD

M.K. Nayak https://orcid.org/000-0003-0220-3760